Proceedings of the 10^{th} Brazilian Congress of Thermal Sciences and Engineering – ENCIT 2004
Braz. Soc. of Mechanical Sciences and Engineering – ABCM, Rio de Janeiro, Brazil, Nov. 29 – Dec. 03, 2004

Paper CIT04-0415

A Study of Trailing-Edge Boundary Condition on the Characteristics of Unsteady Flows over a NACA 0012 Airfoil

Breno Moura Castro
Instituto de Aeronáutica e Espaço - IAE
Praça Mal. Eduardo Gomes, 50 - Jd. das Acácias
CEP: 12228-901 São José dos Campos - SP - Brazil
bmcastro@directnet.com.br

Abstract. *A numerical investigation of the manner in which the trailing-edge boundary condition is implemented is carried out using a Thin-Layer Navier-Stokes code. The Reynolds-averaged equations are solved with a Baldwing-Lomax turbulence model. The unsteady flow simulations were run for a pitch-plunge as well as for a pure-plunge motion. The solutions showed that the trailing-edge boundary condition is not influential for steady-state computations or for oscillations with no dynamic stall. On the other hand, for situations involving dynamic stall, the fine details of the flow field differed quite significantly although the averaged parameters along the cycle were approximately the same.*

keywords: *unsteady, trailing edge, boundary condition, dynamic stall, flapping propulsion.*

1. Introduction

Boundary conditions represent a crucial issue when implementing a solver for both steady and unsteady flow problems. The trailing-edge (TE) boundary condition is no exception, specially for the unsteady case. The boundary condition at the cut of a computational grid can be done implicitly or explicitly. When doing it explicitly, some alternatives exist in the way of implementing the trailing-edge boundary condition. The way of implementing the boundary condition at the trailing-edge of an airfoil can be influential on the characteristics of unsteady flows around this airfoil. This work is carried out to study this influence on the lift and drag coefficient histories of an oscillating NACA 0012 airfoil. Two types of trailing-edge boundary conditions are investigated.

A pitch/plunge combination is imposed to the airfoil with a reduced frequency of 1.0 and half amplitudes of 10 degrees and one chord for the pitch and plunge motions, respectively. The airfoil oscillates around the mid-chord point and the phase angle between the two motions is 90 degrees. The phenomenon of dynamic stall is also an important aspect of unsteady flows. The ability to simulate correctly this phenomenon is a highly desirable feature of a Computational Fluid Dynamics (CFD) solver. Therefore, the influence of the trailing-edge boundary condition implementation on the dynamic stall characteristics is a special concern. Also important is the dynamic-stall boundary for a particular profile. The validity of the NACA 0012 dynamic-stall boundary for the NACA 0014 is investigated in the present work.

The results obtained with the two types of boundary conditions show that they can be influential on the characteristics of unsteady flows over the airfoil depending on the parameter being investigated. If one is interested in quantities that represent an average along the cycle, the TE boundary condition is apparently not influential. On the other hand, the fine details of the flow-field, as the development of the dynamic stall, are strongly affected by the type of TE boundary condition.

2. Theoretical Background

2.1. Governing Equations

The solution for the problem of an unsteady, compressible, and viscous flow of a Newtonian fluid is obtained by solving the Navier-Stokes (N-S) equations. In order to facilitate the numerical solution of the N-S equations, the thin layer approximation is frequently invoked. The Thin-Layer Reynolds-Averaged Navier-Stokes equations are presented in matrix, non-dimensional, and curvilinear coordinate form in Eq. (1):

$$\partial_\tau \hat{Q} + \partial_\xi \hat{F} + \partial_\zeta \hat{G} = Re^{-1} \partial_\zeta \hat{S} \tag{1}$$

where $Q = (\rho, \rho u, \rho w, e)^T$ is the dependent variable and represents a vector which components are the flow state variables, and $\hat{Q} = J^{-1}Q$. The Jacobian of the coordinate transformation from the system (x, z, t) to (ξ, ζ, τ) is $J = (x_\xi z_\zeta - x_\zeta - z_\xi)^{-1}$.

The reference values for non-dimensionalization are the chord length c, the free stream density ρ_∞, the free stream speed-of-sound a_∞, the time c/a_∞, and the specific energy $\rho_\infty a_\infty^2$.

The inviscid and viscous fluxes are given by:

$$\hat{F} = \frac{1}{J}\begin{Bmatrix} \rho U \\ \rho u U + \xi_x p \\ \rho w U + \xi_z p \\ (e+p)U - \xi_t p \end{Bmatrix} \quad \hat{G} = \frac{1}{J}\begin{Bmatrix} \rho W \\ \rho u W + \zeta_x p \\ \rho w W + \zeta_z p \\ (e+p)W - \zeta_t p \end{Bmatrix} \quad \hat{S} = \frac{1}{J}\begin{Bmatrix} 0 \\ \mu m_1 u_\zeta + (\mu/3) m_2 \zeta_x \\ \mu m_1 w_\zeta + (\mu/3) m_2 \zeta_z \\ \mu m_1 m_3 + (\mu/3) m_2 m_4 \end{Bmatrix} \tag{2}$$

where:

$$\begin{aligned} m_1 &= \zeta_x^2 + \zeta_z^2 \\ m_2 &= \zeta_x u_\zeta + \zeta_z w_\zeta \\ m_3 &= \partial_\zeta (u^2 + w^2)/2 + [(\gamma - 1) Pr]^{-1} \partial_\zeta (a^2) \\ m_4 &= \zeta_x u + \zeta_z w \end{aligned} \tag{3}$$

The terms ξ_x, ξ_z, ξ_t, ζ_x, ζ_z, and ζ_t are the metrics of the coordinate transformation. U and W are the contravariant velocity components given by:

$$\begin{aligned} U &= \xi_t + \xi_x u + \xi_z w \\ W &= \zeta_t + \zeta_x u + \zeta_z w \end{aligned} \tag{4}$$

Pressure is related to the other variables through the equation of state for an ideal gas:

$$p = (\gamma - 1)\left[e - \rho(u^2 + w^2)/2\right] \tag{5}$$

2.2. Numerical Technique

The Thin-Layer Navier-Stokes (TLNS) equations are discretized using an alternate direction implicit (ADI), third-order accurate in space, second-order accurate in time, finite-volume scheme, which can be represented by:

$$\begin{aligned} &\left[I + h_\xi (\nabla_\xi \hat{A}^+_{i,k} + \Delta_\xi \hat{A}^-_{i,k})^p\right] \Delta \hat{Q}^*_{i,k} = -\hat{r}^p_{i,k} \\ &\left[I + h_\zeta (\nabla_\zeta \hat{B}^+_{i,k} + \Delta_\zeta \hat{B}^-_{i,k} - Re^{-1} \delta_\zeta \hat{M}_{i,k})^p\right] (\hat{Q}^{p+1}_{i,k} - \hat{Q}^p_{i,k}) = \Delta \hat{Q}^*_{i,k} \end{aligned} \tag{6}$$

where:

$$\begin{aligned} \hat{r}^p_{i,k} = \quad & (\hat{Q}^p_{i,k} - \hat{Q}^n_{i,k}) + h_\xi (\hat{F}_{i+1/2,k} - \hat{F}_{i-1/2,k})^p \\ & + h_\zeta (\hat{G}_{i,k+1/2} - \hat{G}_{i,k-1/2})^p - Re^{-1} h_\zeta (\hat{S}_{i,k+1/2} - \hat{S}_{i,k-1/2})^p \end{aligned} \tag{7}$$

The variables $\hat{A}$, $\hat{B}$, and $\hat{M}$ are the flux Jacobian matrices and are defined as $\hat{A} = \partial \hat{F}/\partial \hat{Q}$, $\hat{B} = \partial \hat{G}/\partial \hat{Q}$, and $\hat{M} = \partial \hat{S}/\partial \hat{Q}$, respectively. A flux splitting (Steger and Warming, 1981) is applied to matrices $\hat{A}$ and $\hat{B}$, where $\hat{A} = \hat{A}^+ + \hat{A}^-$ and $\hat{B} = \hat{B}^+ + \hat{B}^-$.

The h quantities are defined as $h_\xi = \Delta\tau/\Delta\xi$ and $h_\zeta = \Delta\tau/\Delta\zeta$. ∇, Δ, and δ are the forward, backward, and central difference operators, respectively.

The variables $\hat{F}_{i+1/2,k}$, $\hat{G}_{i,k+1/2}$, and $\hat{S}_{i,k+1/2}$ are numerical fluxes. The superscript $(.)^n$ denotes the physical time step and the superscript $(.)^p$ is related to Newton sub-iterations within each physical time step, which are used to improve time accuracy. These sub-iterations minimize the linearization and factorization errors and help drive the left-hand side of Eq. (6) to zero.

Inviscid numerical fluxes, $\hat{F}_{i+1/2,k}$ and $\hat{G}_{i,k+1/2}$, are evaluated by means of the Osher's third-order accurate, upwind-biased scheme (Chakravarthy and Osher, 1983). Linearization of the left-hand side of Eq. (6) is performed by evaluating the flux Jacobian matrices, $\hat{A}$ and $\hat{B}$, with the Steger and Warming flux-vector splitting (Steger and Warming, 1981). The viscous numerical flux $\hat{S}_{i,k+1/2}$ is computed with second-order central differences. Furthermore, a Total Variation Diminishing (TVD) flux limiter (Rai and Chakravarthy, 1986) is applied to minimize numerical oscillations at shocks developed at transonic speeds.

2.3. Boundary Conditions

For inviscid flow solutions, the viscous terms on the RHS of Eq. (1) are set to zero, and the flow-tangency boundary condition is used at the surface of the airfoil. For Navier-Stokes solutions, the no-slip condition is applied. Density and pressure are extrapolated to the surface for both Euler and Navier-Stokes solutions.

Inflow and outflow boundary conditions are imposed at the farfield boundaries. For the inflow boundary, flow properties such as pressure, temperature, and velocity are specified while the density is extrapolated from the neighbor interior

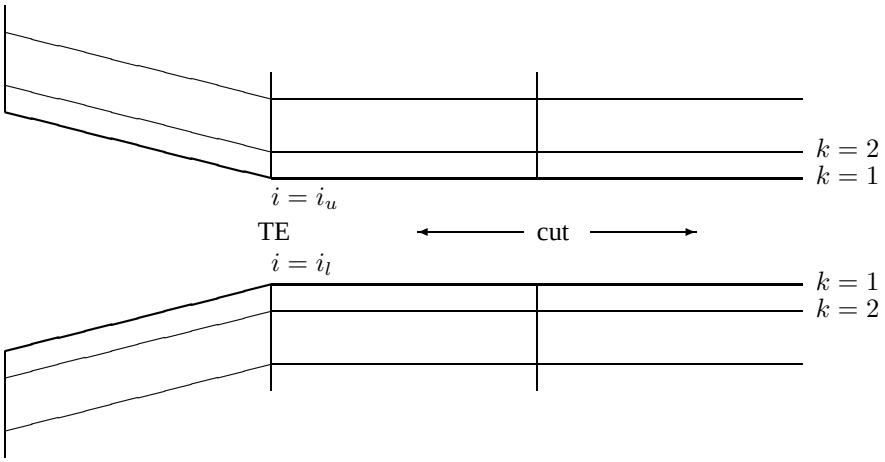

Figure 1: Schematic of a C-grid near the trailing edge

points. Pressure is specified for the outflow boundary condition and all other properties are extrapolated from the interior. Extrapolations in both cases are performed by using Riemann invariants.

For unsteady motions, the flow-tangency and no-slip conditions are modified to include the local motion of the airfoil, which also contributes to the pressure on the surface. Therefore, the momentum equation normal to the surface (ζ direction) is solved to predict the pressure for a viscous flow more accurately

$$\partial_\zeta p|_{wall} = -\frac{1}{\nabla^2 \zeta}\left[\rho \partial_t \left\{ \begin{array}{c} \dot{x}|_{wall} \\ \dot{y}|_{wall} \end{array} \right\} \cdot \nabla\zeta + \partial_\zeta \rho|_{wall} \nabla\xi \cdot \nabla\zeta\right] \tag{8}$$

where $\dot{x}|_{wall}$ and $\dot{y}|_{wall}$ are the components of the airfoil velocity. Furthermore, $\nabla\xi \cdot \nabla\zeta = 0$ when assuming that the grid is orthogonal at the surface. If the airfoil is stationary, the normal pressure gradient vanishes in agreement with boundary-layer theory.

2.3.1. Trailing Edge Boundary Condition

The trailing edge (TE) boundary condition is a crucial issue in both steady-state and unsteady computations. A schematic of a C-grid near the trailing edge is shown in Fig. 1. The cut is the region of the computational domain corresponding to points for which $(1 \leq i \leq i_l, k = 1)$ and $(i_u \leq i \leq i_{max}, k = 1)$. These points are coincident in the physical domain. The trailing edge point in the physical domain corresponds to the points $(i = i_l)$ and $(i = i_u)$ in the computational domain. The points along the cut, including the trailing edge, are shown separated in Fig. 1 just for clarity.

The boundary condition at the cut of a C-grid can be done either explicitly or implicitly. In the present method, this boundary condition is computed explicitly, after the flow tangency or the no-slip condition is applied to the surface of the airfoil. The flow variables at the cut, $k = 1$, are calculated by averaging the upper and lower neighboring points for $k = 2$. Some options exist when one must decide how to implement the explicit boundary condition at the trailing edge. Three possibilities for this implementation exist:

- use the averaged value from points at $(i_u, 2)$ and $(i_l, 2)$;
- treat the trailing edge as two different points (no averaging);
- use the averaged value from points at $(i_u, 1)$ and $(i_l, 1)$.

The first option is the most obvious because it is just an extension of the boundary condition applied at the cut of the C-grid. However, the first option is not the most suitable one because it does not enforce the no-slip or the flow-tangency condition at the trailing edge. These boundary conditions are overwritten when computing the average of the off-surface points ($k = 2$). In this work, the second alternative is called the "free TE boundary condition." The no-slip or the flow-tangency condition is applied to the TE. However, because the TE is treated as two different points in the computational domain, a discontinuity may occur at the TE since the two points are the same in the physical domain. The last option, called averaged TE, appears to be the most consistent one for the present work because, in terms of discretization of the physical domain, the points of the cut corresponding to the TE are the same. Furthermore, it is guaranteed that the no-slip

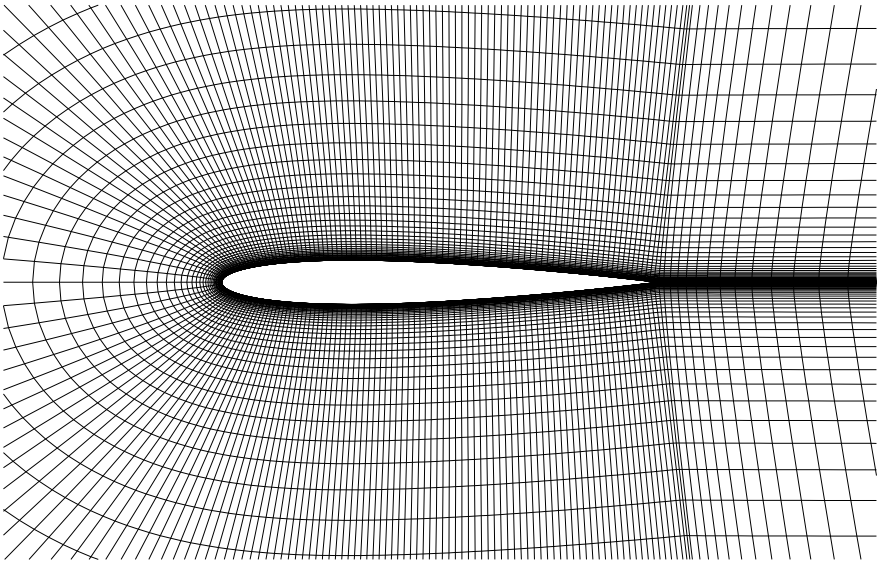

Figure 2: Grid around the NACA 0012 airfoil

condition or the flow-tangency condition is maintained at the TE since these conditions are applied for $k = 1$ before averaging.

3. Results and Discussion

The influence of applying the free or the averaged TE is investigated. A single NACA 0012 airfoil oscillating in a combined pitch and plunge motion is used to determine the difference in the solutions for both TE conditions. The reduced frequency of the motion is defined as $\kappa = \omega c/U_\infty$, where ω is the frequency, c corresponds to the chord of the airfoil, and U_∞ represents the free stream velocity. The reduced frequency is set to $\kappa = 1.0$ and the pitch and plunge half amplitudes are $\hat{\alpha} = 10$ degrees and $\hat{h} = 1.0$, respectively. Pitch leads plunge by $\phi = 90$ degrees. The pivot point for the pitch motion is chosen to be the half chord or $x_p = 0.5$. The free-stream Mach and Reynolds numbers are $M_\infty = 0.3$ and $Re_\infty = 10^6$, respectively. The B-L turbulence model is applied for the fully turbulent computations. The C-grid is presented in Fig. 2 and its dimensions are $i_{max} = 281$ and $k_{max} = 81$.

The non-dimensional equations of motion are given by:

$$h = \hat{h}\,\sin(M_\infty \kappa \tau) \qquad \alpha = \hat{\alpha}\,\sin(M_\infty \kappa \tau + \phi) \tag{9}$$

Steady-state computations are performed for $\alpha = 0$ degrees, employing both the averaged and free TE boundary conditions. The pressure distributions over the surface of the airfoil are presented in Fig. 3. The match is extremely good for the two solutions. However, no conclusion is drawn from the steady-state case because the flow is symmetric, and this might be the reason for the excellent match.

The motion parameters for the oscillation of the airfoil have been chosen because they force a relatively high induced angle of attack, therefore, allowing dynamic stall to occur. The time history of the aerodynamic coefficients is presented in Fig. 4 for both types of boundary conditions. Clearly, the solution is not periodic. For the same type of boundary condition, the curve for the lift coefficients, for example, does not behave periodically.

The pressure distributions for various positions along the cycle are shown in Fig. 5. The left-hand side of this figure corresponds to positions along the up stroke and the right-hand side to the down stroke. Although some pressure distributions are not in close agreement for the two TE conditions, the development of the dynamic stall is not dramatically different. In order to better clarify this point, entropy contours during the upstroke part of the motion of the airfoil are shown in Fig. 6. The vortices generated during the motion are well captured. The left-hand side of Fig. 6 represents the averaged TE boundary condition. The free TE boundary condition is represented on the right-hand side. Although the vortices do not match perfectly for the two types of TE boundary condition, their sizes are comparable and the speed with which they convect downstream is approximately the same. Note, also, that the flow is not periodic. This can be seen in Fig. 7 in which the variation of the drag coefficient is shown against the lift coefficient. Clearly, the solution is not

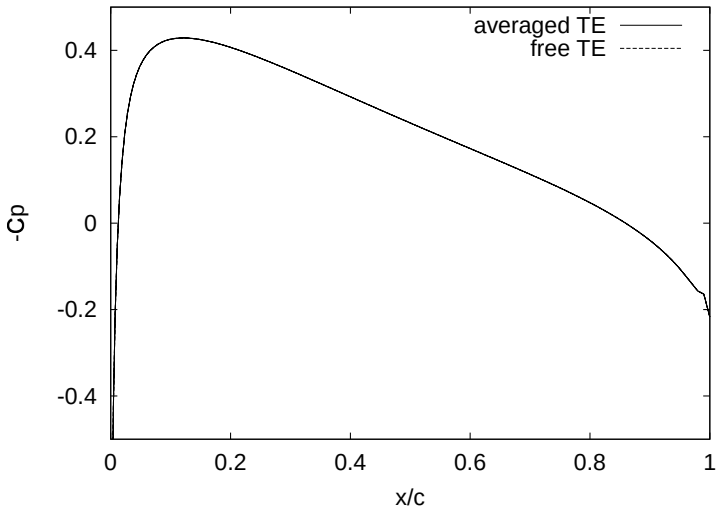

Figure 3: Steady-state solutions for averaged and free TE

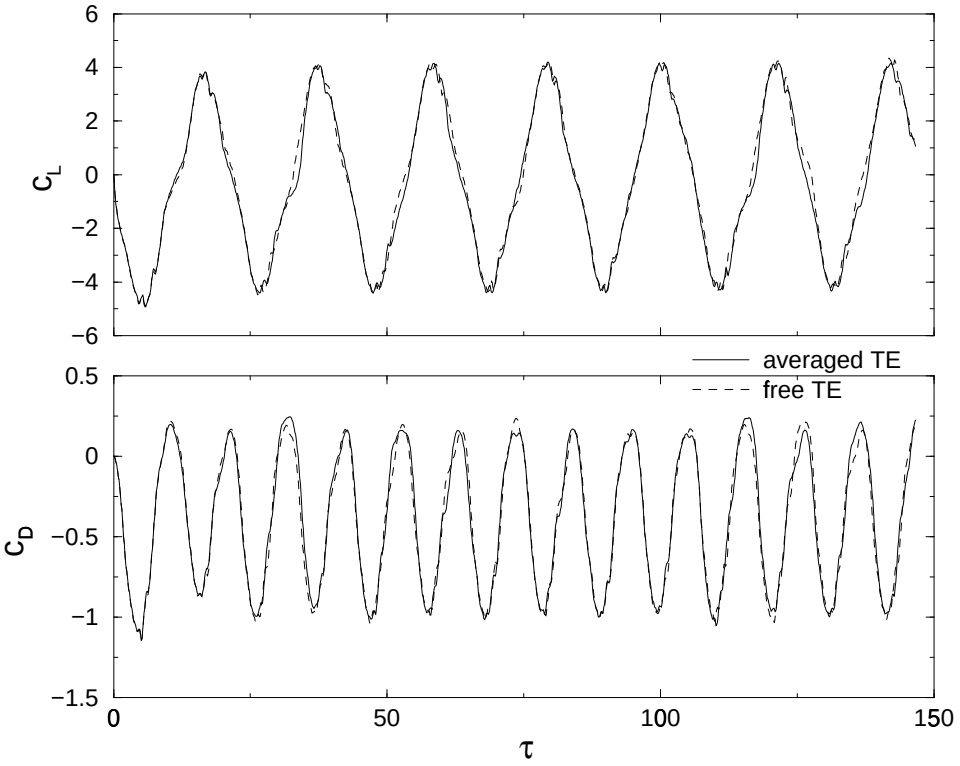

Figure 4: History of lift and drag coefficients for the pitch/plunge case

periodic. However, it stays inside a confined area although it wanders from place to place in that area. This behavior is represented in the Chaos Theory by the Torus Attractor (Castro, 2001). This attractor appears to be the same for both types of TE boundary condition. Furthermore, a computation of the thrust coefficient and propulsive efficiency showed that these parameters are virtually the same for both TE conditions ($c_T = 0.40$ and $\eta = 0.21$). As a conclusion from this case, the type of TE boundary condition is apparently not influential when one is interested in quantities that represent an average along the cycle. On the other hand, the fine details of the flow-field, as the development of the dynamic stall, are strongly affected by the type of boundary condition at the trailing edge.

A case with no dynamic stall was also run to evaluate the TE boundary condition. A NACA 0014 airfoil oscillating in pure plunge is computed. The reduced frequency of the motion is $\kappa = 0.4$ with a half amplitude of $\hat{h} = 0.4$. The free-stream Mach and Reynolds numbers are $M = 0.3$ and $Re = 10^6$, respectively. The flow is assumed fully turbulent and the B-L turbulence model is used. The domain is discretized by a 321×91 C-grid shown in Fig. 8.

When steady-state computations are performed, they deliver the same solution for both types of TE boundary condition. This is similar to the NACA 0012 airfoil case. Unsteady simulations are also computed for the two types of TE boundary condition. The history of the unsteady lift and drag aerodynamic coefficients is presented in Fig. 9. The agreement between the solutions for the two different boundary conditions is quite good. The thrust coefficient is $c_T = 0.041$ and the propulsive efficiency is $\eta = 0.73$ for both cases. Therefore, in situations where there is no dynamic stall, the difference of applying an averaged TE or a free TE boundary condition is negligible.

Although dynamic stall was computed somewhat differently for the two types of TE boundary condition, the effect on the predicted thrust coefficient, the propulsive efficiency, and the convection speed of the dynamic vortices was minimal. Therefore, the averaged TE boundary condition is used throughout the course of this work.

Another important computation with the averaged TE boundary condition was performed to assess the influence of this boundary condition on the dynamic-stall boundary suggested by Tuncer (Tuncer et al., 1998). They computed the unsteady flow over a NACA 0012 airfoil oscillating in pure plunge and varied the reduced frequency and the amplitude of the motion to determine the onset of dynamic stall. Their computations, using a free TE boundary condition, showed that the dynamic-stall boundary is given by the equation:

$$\hat{h}\kappa = 0.35 \tag{10}$$

Two computations with $\kappa = 1.0$ were performed for $\hat{h} = 0.3$ and $\hat{h} = 0.4$. The first, corresponding to $\hat{h}\kappa = 0.3$, predicted no separation of the flow, in agreement with the dynamic stall boundary given by Eq. 10. The second, corresponding to $\hat{h}\kappa = 0.4$, calculated a separated flow during the motion of the airfoil, confirming that the averaged TE boundary condition also delivers the dynamic-stall boundary described by Eq. 10.

A second set of computations was performed for the averaged TE boundary condition but, this time, for the NACA 0014 airfoil. The objective was to determine the influence of the shape of the airfoil on the dynamic-stall boundary represented by Eq. 10. The reduced frequency was kept equal to $\kappa = 1.0$ while the amplitude of the pure plunge motion, $\hat{h}$, was varied. For $\hat{h} = 0.4$, no separation of the flow was predicted, suggesting that the dynamic-stall boundary might have changed for the NACA 0014 airfoil. A computation with $\hat{h} = 0.5$ showed that the flow was detached from the airfoil surface. These computations are shown schematically in Fig. 10, along with the dynamic-stall boundary of Eq. 10. Therefore, clearly, the shape of the airfoil has a significant influence on the onset of dynamic stall. For the NACA 0014, the dynamic-stall boundary should be further investigated and it appears that it will be given by:

$$\hat{h}\kappa \geq 0.4 \tag{11}$$

4. Concluding Remarks

A study of the trailing-edge boundary condition was carried out in the present work. A computational code based on the Thin-Layer Navier-Stokes equations was used. Two types of TE boundary conditions were defined and investigated for a NACA 0012 oscillating in both a pitch-plunge and a pure-plunge motions. Some simulations involving a NACA 0014 oscillating in pure plunge were also performed.

For the pitch-plunge motion, the pivot point was set to be the half chord, the reduced frequency to $\kappa = 1.0$, the half amplitudes to $\hat{h} = 1.0$ and $\alpha = 10$ degrees, and the phase angle to $\phi = 90$ degrees. The parameter combination is such that dynamic stall is forced. The two different types of TE boundary conditions, namely the free and the averaged boundary conditions, delivered the same solution for a steady-state simulation. For the dynamic-stall case, the solutions do not match perfectly, differing on the fine details of the flow. However, they stayed inside a confined area which appears to be a Torus Attractor of the Chaos Theory. The averaged quantities along the cycle were not influenced by the TE condition.

The pure-plunge computations with no dynamic stall showed that the different TE boundary conditions yielded virtually the same solution for a NACA 0014, reduced frequency of $\kappa = 0.4$, and half amplitude of $\hat{h} = 0.4$. Furthermore, the difference between the averaged parameters was negligible.

The dynamic-stall boundary for the NACA 0014 was found to be different from $\hat{h}\kappa = 0.35$ for the NACA 0012. Consequently, the dynamic-stall boundary for the NACA 0014 should be further investigated.

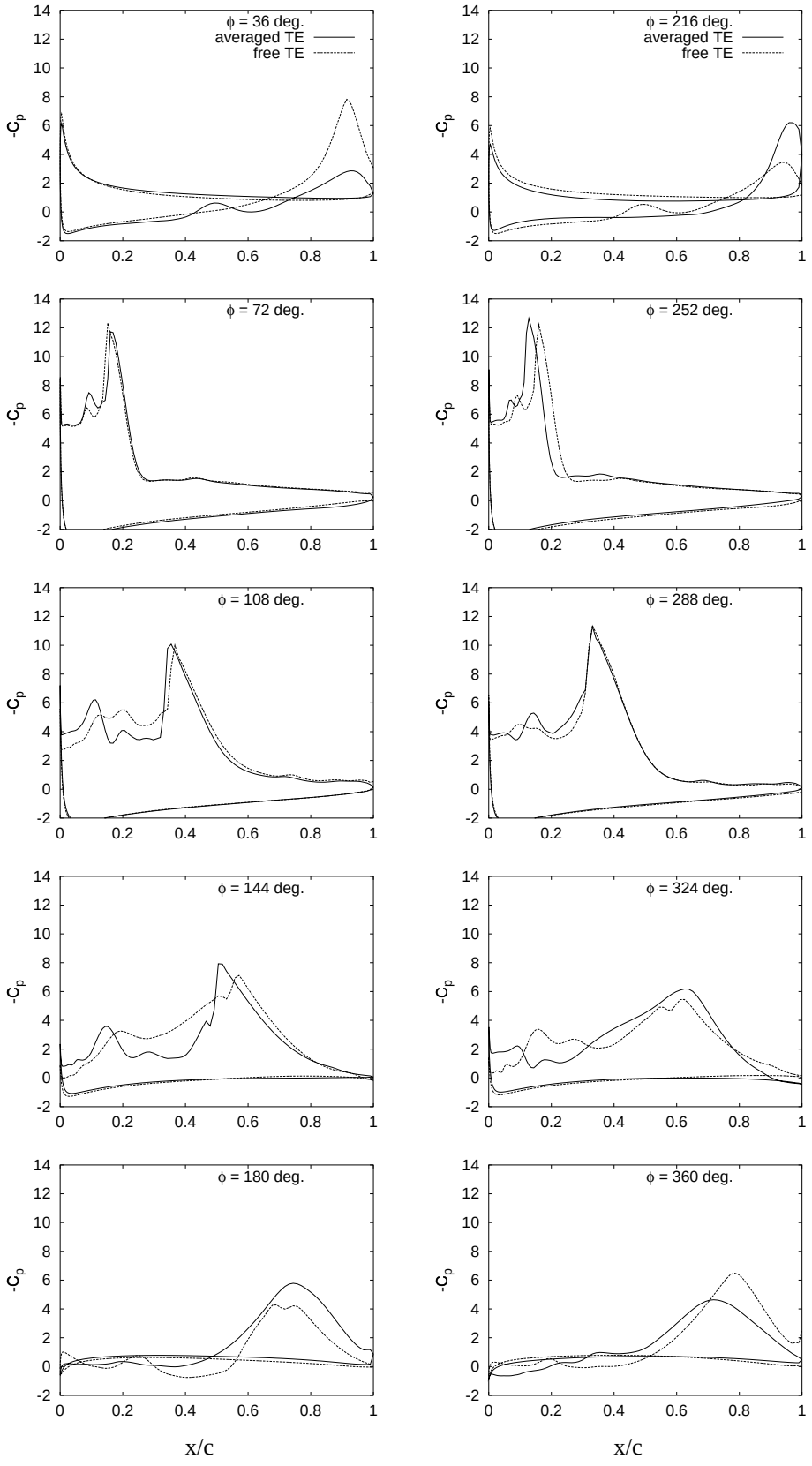

Figure 5: Comparison of pressure distributions for averaged and free TE

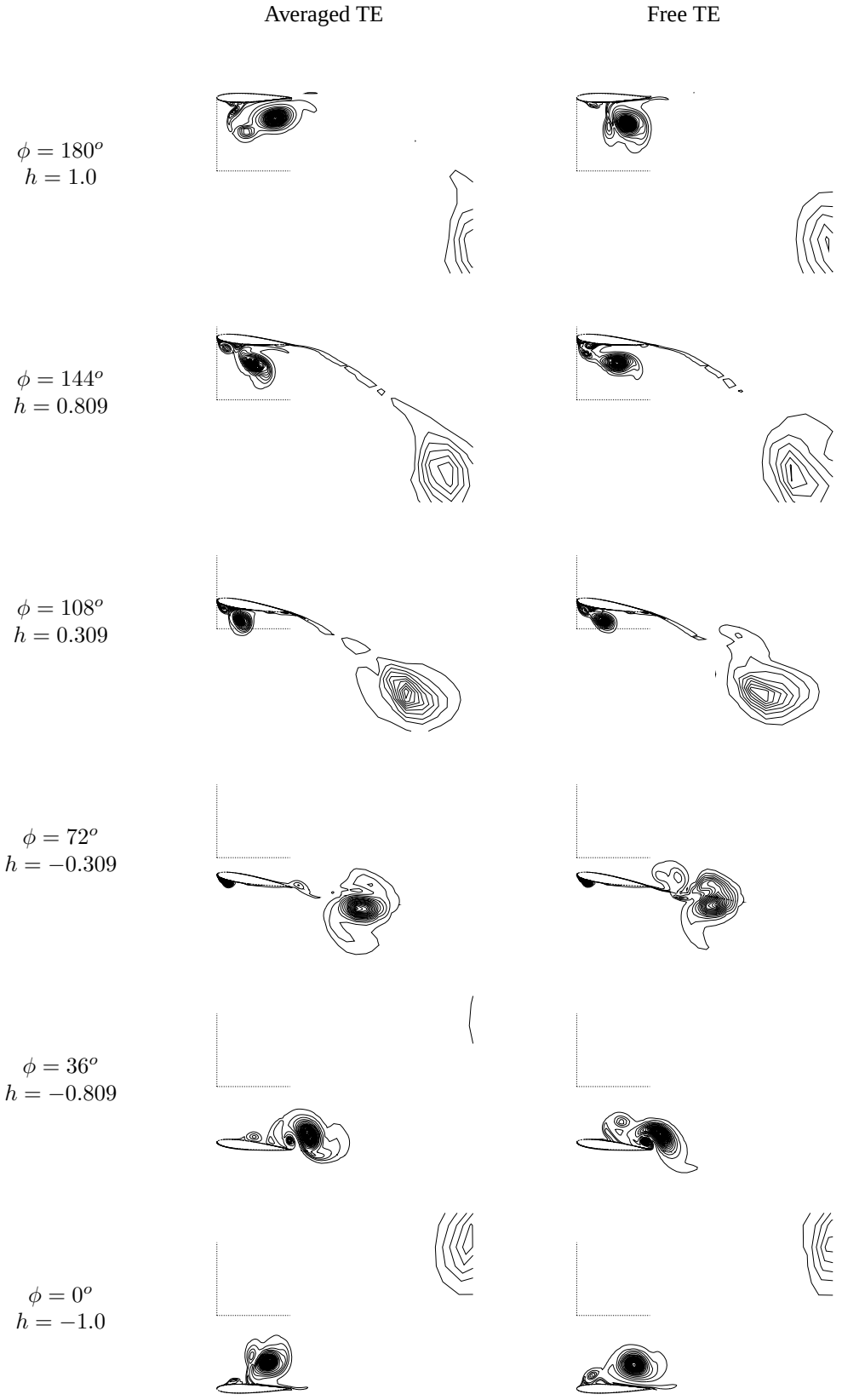

Figure 6: Comparison of pressure distributions for averaged and free TE, NACA 0012, $\hat{\alpha} = 10^o$, $M_\infty = 0.3$, $k = 1$, $Re_\infty = 1 \times 10^6$

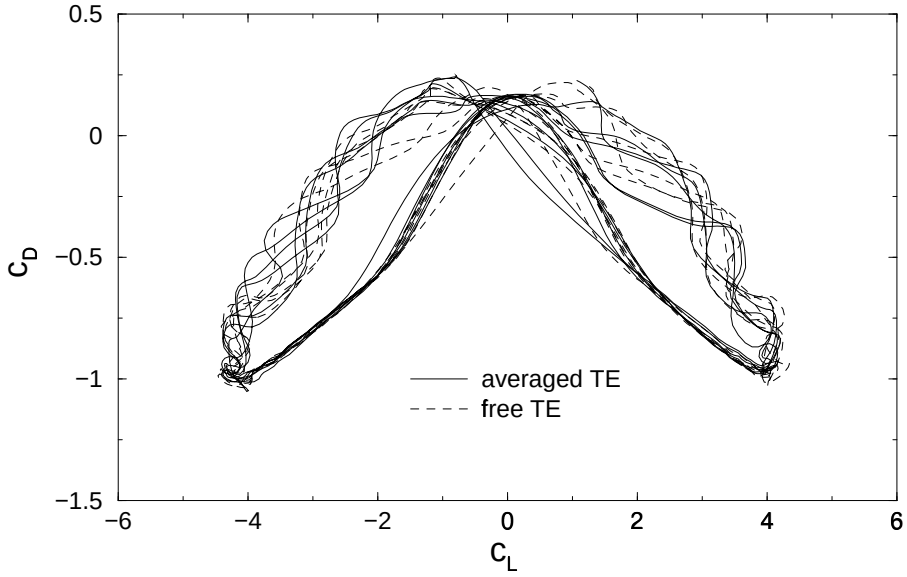

Figure 7: Variation of c_D against c_L for the pitch/plunge case

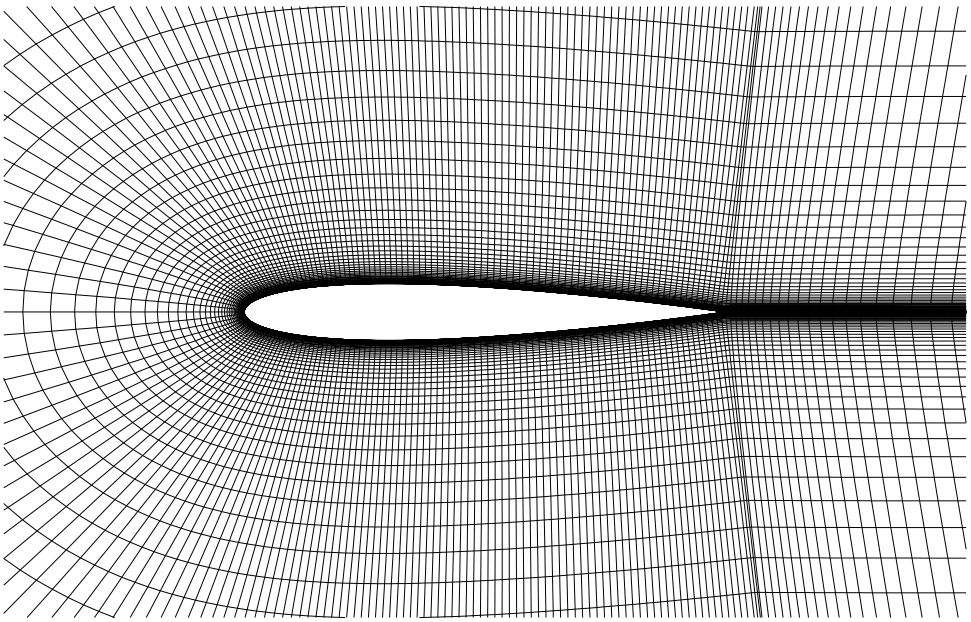

Figure 8: Grid around the NACA 0014 airfoil

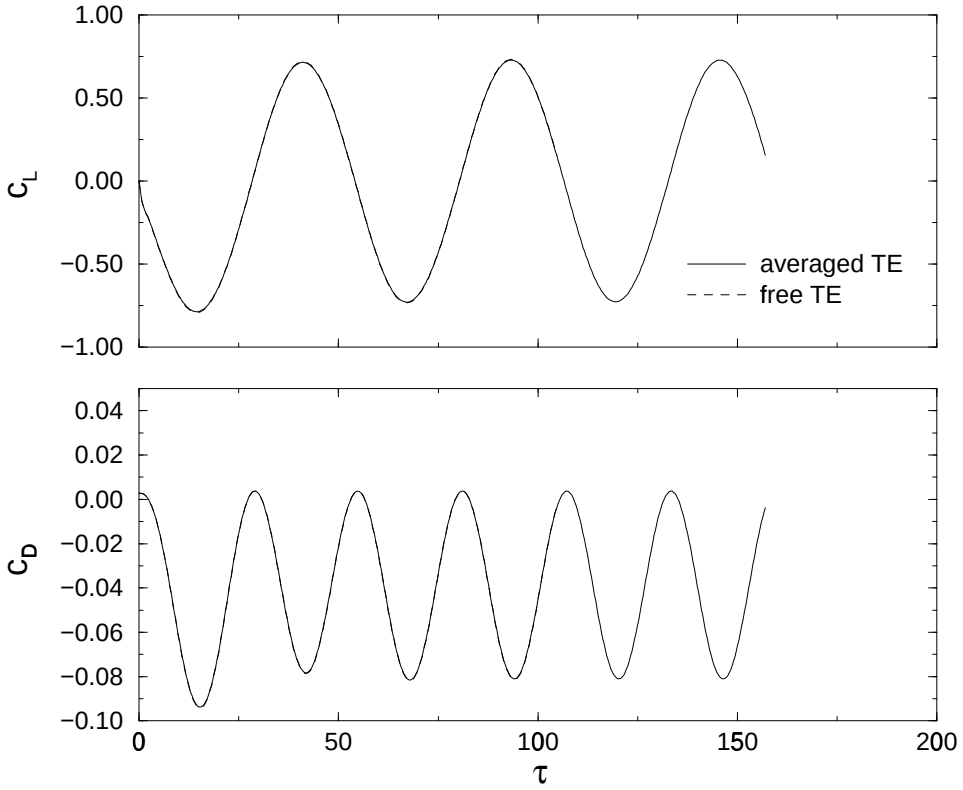

Figure 9: History of lift and drag coefficients for the pure plunge case

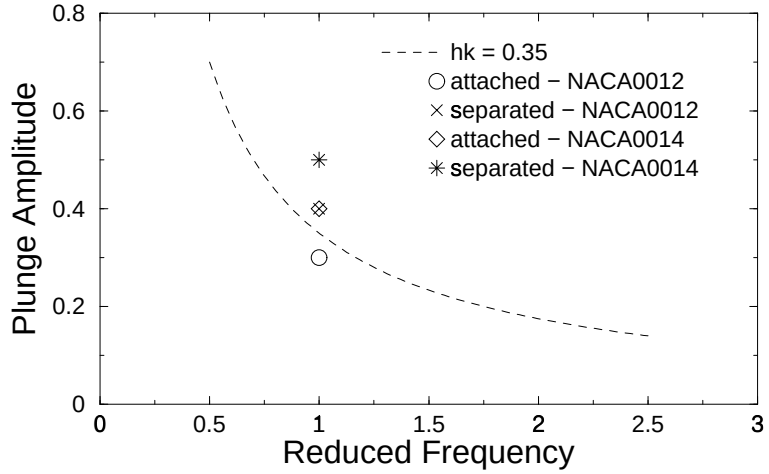

Figure 10: Dynamic-stall boundary for the NACA 0012 airfoil

5. References

Castro, B. M., 2001, “Multi-Block Parallel Navier-Stokes Simulation of Unsteady Wind Tunnel and Ground Interference Effects”, PhD thesis, Naval Postgraduate School, Monterey, CA.

Chakravarthy, S. R. and Osher, S., 1983, Numerical Experiments with the Osher Upwind Scheme for the Euler Equations, “AIAA Journal”, Vol. 21, No. 9, pp. 1241–1248.

Rai, M. M. and Chakravarthy, S. R., 1986, An Implicit Form for the Osher Upwind Scheme, “AIAA Journal”, Vol. 24, No. 5, pp. 735–743.

Steger, J. L. and Warming, R. F., 1981, Flux Vector Splitting of the Inviscid Gasdynamic Equations with Application to Finite-Difference Methods, “Journal of Computational Physics”, Vol. 40, pp. 263–293.

Tuncer, I. H., Walz, R., and Platzer, M. F., 1998, A Computational Study on the Dynamic Stall of a Flapping Airfoil, “16th AIAA Applied Aerodynamics Conference”, pp. 219–225. Albuquerque, New Mexico.